Eric Marsh[1]
e-mail: emarsh@psu.edu

Jeremiah Couey

Pennsylvania State University,
21 Reber Building,
University Park, PA 16802

Ryan Vallance
George Washington University,
738 Phillips Hall,
802 22nd Street N.W.,
Washington, D.C. 20052

Nanometer-Level Comparison of Three Spindle Error Motion Separation Techniques

This work demonstrates the state of the art capabilities of three error separation techniques for nanometer-level measurement of precision spindles and rotationally-symmetric artifacts. Donaldson reversal is compared to a multi-probe and a multi-step technique using a series of measurements carried out on a precision aerostatic spindle with a lapped spherical artifact. The results indicate that subnanometer features in both spindle error motion and artifact form are reliably resolved by all three techniques. Furthermore, the numerical error values agree to better than one nanometer. The paper discusses several issues that must be considered when planning spindle or artifact measurements at the nanometer level. [DOI: 10.1115/1.2118747]

Introduction

Higher accuracy manufacturing and metrology methods have shrunk tolerances by three orders of magnitude since the 1940s [1]. Today, some ultraprecision systems require workpiece tolerances with nanometer-level form error and subnanometer surface finish. The rotary bearings and spindles used in machines and metrology instruments are critical to achieving such tolerances and finishes because any deviation from pure rotation decreases accuracy [2,3]. For example, asynchronous (nonrepeatable) error motion in computer hard disk drives (HDD) limits the density of data storage, even though typical HDD error motions are already less than 100 nm [4].

An entire field of research has grown from the need to accurately quantify spindle performance. Tlusty, Bryan, and Donaldson inspired four decades of work to reduce the uncertainty of spindle and roundness measurements through clever hardware developments and analysis [2,3,5]. Sensors, data acquisition, structural design, and technique are now the principal limits on uncertainty [6–9].

Accurate and reliable measurement of submicrometer spindle error motions is complicated since the measurement involves a target that will inevitably have its own imperfections. A spindle measurement includes the contribution from both the spindle error and the form error of this target surface. For high precision aerostatic spindles, the form error of even an optical quality, lapped artifact cannot be neglected.

The literature documents several techniques to separate the spindle error motion from the artifact form error. For example, Donaldson reversal unambiguously separates the entire artifact form error from the spindle error motion [5]. The literature describes other separation methods including multistep techniques where measurements are recorded with a displacement sensor targeting an artifact at a number of equally-spaced angular orientations and multi-probe techniques where measurements are simultaneously recorded from multiple sensors [10–16]. These multi-position (i.e., multi-step and multi-probe) techniques are not true reversals, however. As Whitehouse and others point out, the multi-step and multi-probe methods are insensitive to (i.e., do not accurately separate) some harmonic components of the error motion that are predictable functions of the number and positioning of the displacement sensors [17]. However, these multi-position techniques remain useful when used with a proper understanding of their limitations.

The steps required to measure the spindle error motion and the form error of an artifact are shown diagrammatically in Fig. 1. First, the data from a displacement sensor is analog antialias filtered and digitized at evenly spaced intervals of the spindle's angular rotation. Additional low and high pass filtering may be applied to remove the effects of structural vibration and thermal drift, respectively. Furthermore, the fundamental harmonic component is removed for all but axial error measurements since this component is changed arbitrarily by recentering the artifact on the spindle and is therefore not part of spindle error motion or artifact form error.

The data are collected for a suitable number of spindle revolutions to reduce the measurement uncertainty. The exact number is chosen on a case-by-case basis by the metrologist [8]. The average, or synchronous, measurement is the mean contour calculated from the multiple revolutions of data and it is mathematically equivalent to the integer components of the data in the Fourier domain. The remaining data are the asynchronous component and correspond to the noninteger components in the Fourier domain, as shown in Fig. 1. A stable artifact has no asynchronous contribution, so the asynchronous information is necessarily attributed to some unknown combination of spindle error motion, structural vibration, instrument noise, thermal drift, and other effects. Only the synchronous component of the measured data is considered during the error separation process. It is important to recognize that the synchronous data will still include the influence of defects other than the spindle that happen to be synchronous with its rotation (e.g., motor cogging, forced vibration, etc.).

The calculations to separate spindle error from artifact form error require multiple measurements. For each component of error motion (e.g., radial, tilt, face), Donaldson reversal requires two measurements, multi-probe methods require three or more measurements, and the multi-step technique often requires eight or more (chosen by the metrologist). The error motion of a spindle's axis of rotation is characterized by five degrees of freedom (the sixth degree of freedom is the desired rotation). Therefore, a complete characterization of a spindle requires four applications of any of the error separation techniques used in this paper, plus one additional measurement in the axial direction, which does not require error separation. For example, a complete spindle error motion characterization by Donaldson reversal requires four radial and/or face reversals, each made using two measurements, plus the axial measurement for a total of nine measurements.

In this work, we demonstrate the capability of three error sepa-

[1]Author to whom correspondence should be addressed.

Contributed by the Manufacturing Engineering Division of ASME for publication in the JOURNAL OF MANUFACTURING SCIENCE AND ENGINEERING. Manuscript received December 19, 2004; final manuscript received April 21, 2005. Review conducted by T. R. Kurfess.

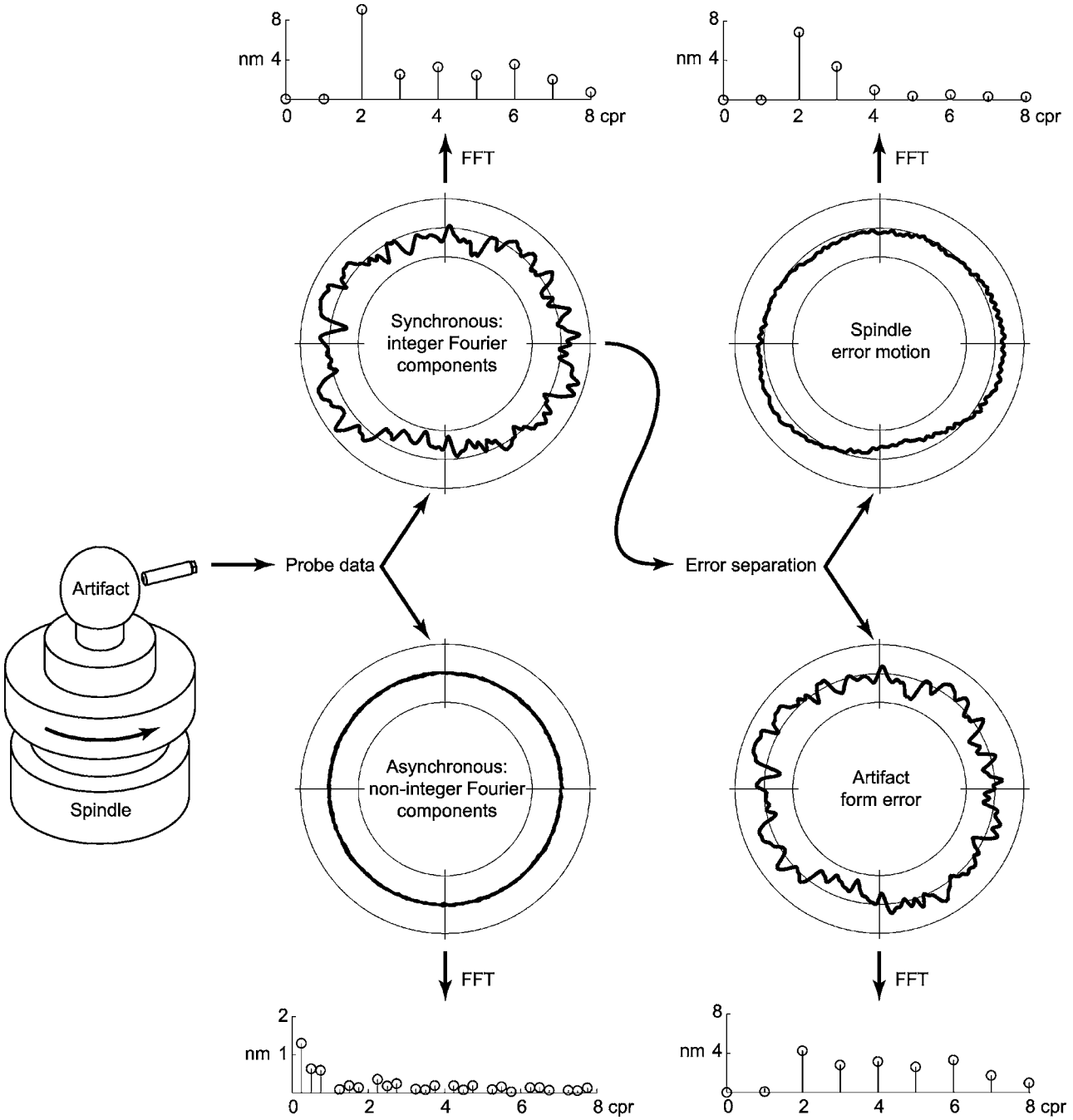

Fig. 1 Separation of spindle error motion and artifact form error from displacement measurement data

ration methods at the nanometer level using radial measurements. We also describe developments in experimental technique that allow spindle error and roundness measurements with subnanometer repeatability. To achieve this, we have implemented the error separation methods with a slight modification; we reorient (rotate) the spindle under test relative to the sensor rather than move the sensor. This modification is critical to achieving subnanometer repeatability because the accuracy of all separation methods is degraded by imperfectly repositioned sensors or by using multiple displacement sensors of unequal sensitivity. With the benefit of the rotary table modification, and with the understanding that some error separation methods do not accurately separate all components, the three methods agree within one nanometer.

Error Separation Techniques

Measuring either the error motion of a precision spindle or the form error of a rotationally symmetric workpiece is essentially the same task because in both cases the displacement sensor measures a combination of the spindle error motion and workpiece form error [2]. Today's externally pressurized aerostatic and hydrostatic spindles show the same nanometer-level error motion as many of the precision workpieces that need to be measured; neither contributor can be ignored.

Complete and accurate separation requires that all periodic harmonics in the recorded data be properly attributed to spindle error motion or artifact form error in the correct proportion. Reversal

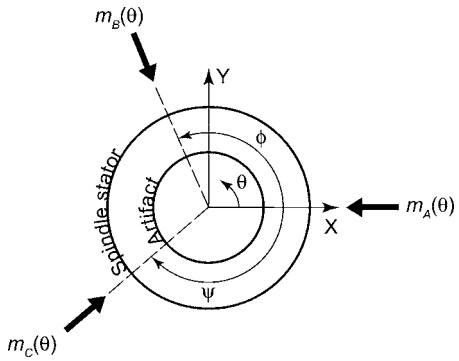

Fig. 2 Schematic of the three-probe error separation method (after Mitsui [20])

methods, proposed by Donaldson and Estler [18,19], result in complete separation of the workpiece form errors from the spindle error motion. This allows the metrologist to obtain reliable information without the need for comparison with master artifacts maintained by national standards laboratories.

Multi-probe and multi-step methods are considered error separation techniques rather than true reversals as mentioned earlier and described in the sections that follow. These multi-position techniques do not completely separate the errors from spindle and workpiece, but are still used in certain situations. Evans, Hocken, and Estler provide a comprehensive review of error separation techniques and point out the underlying differences, limitations and similarities [19]. Both classes of multi-position methods (i.e., multi-step and multi-probe) model errors with a Fourier series, use redundant measurements for the benefit of averaging, and use circle closure to reduce the measurement uncertainty.

Multi-Probe Error Separation. Whitehouse published detailed analyses of the capability of multi-probe error separation using three or more displacement sensors targeting an artifact [17]. Figure 2 shows a schematic of the measurement with three displacement sensors that simultaneously record $m_A(\theta)$, $m_B(\theta)$, and $m_C(\theta)$. Sensors B and C are separated in the fixed (nonrotating) XY plane from sensor A by angles ϕ and ψ, respectively.

As shown in Eqs. (1)–(3), the measurements recorded by the three displacement sensors are a summation of the part roundness $P(\theta)$, including a phase shift due to sensor location, and the $x(\theta)$ and $y(\theta)$ components of the spindle error motion,

$$m_A(\theta) = P(\theta) + x(\theta) \tag{1}$$

$$m_B(\theta) = P(\theta - \phi) + x(\theta)\cos\phi + y(\theta)\sin\phi \tag{2}$$

$$m_C(\theta) = P(\theta + \psi) + x(\theta)\cos\psi - y(\theta)\sin\psi \tag{3}$$

$M(\theta)$ is defined as a linear combination of the three distinct measurements using coefficients of unity, a, and b, as shown in Eq. (4). The unknown coefficients a and b are determined by solving Eqs. (5) and (6) simultaneously.

$$M(\theta) = m_A(\theta) + am_B(\theta) + bm_C(\theta) \tag{4}$$

$$a\cos\phi + b\cos\psi + 1 = 0 \tag{5}$$

$$a\sin\phi - b\sin\psi = 0 \tag{6}$$

The roundness of the artifact is modeled as an infinite Fourier series

$$P(\theta) = \sum_{k=1}^{\infty} (A_k \cos k\theta + B_k \sin k\theta) \tag{7}$$

Equation (8) shows the result when the series representation for the artifact roundness $P(\theta)$ is substituted into the summed measurement $M(\theta)$, angle addition trigonometry identities are applied, and common terms of $A_k \cos k\theta$, $A_k \sin k\theta$, $B_k \cos k\theta$, and $B_k \sin k\theta$ are collected.

$$\begin{aligned} M(\theta) &= m_A(\theta) + am_B(\theta) + bm_C(\theta) \\ &= \sum_{k=1}^{\infty} A_k(1 + a\cos k\phi + b\cos k\psi)\cos k\theta \\ &\quad + \sum_{k=1}^{\infty} A_k(a\sin k\phi - b\sin k\psi)\sin k\theta \\ &\quad + \sum_{k=1}^{\infty} B_k(1 + a\cos k\phi + b\cos k\psi)\sin k\theta \\ &\quad + \sum_{k=1}^{\infty} B_k(b\sin k\psi - a\sin k\phi)\cos k\theta \end{aligned} \tag{8}$$

At this point, $\alpha_k = 1 + a\cos k\phi + b\cos k\psi$ and $\beta_k = b\sin k\psi - a\sin k\phi$ may be computed, so the remaining step is to compare the terms of Eq. (8) to the Fourier coefficients of $M(\theta)$ [F_k and G_k, as defined in Eq. (9)] to determine A_k and B_k. Therefore, Eq. (10) is solved for each term in the Fourier series,

$$M(\theta) = \sum_{k=1}^{\infty} (F_k \cos k\theta + G_k \sin k\theta) \tag{9}$$

$$\begin{bmatrix} \alpha_k & \beta_k \\ -\beta_k & \alpha_k \end{bmatrix} \begin{Bmatrix} A_k \\ B_k \end{Bmatrix} = \begin{Bmatrix} F_k \\ G_k \end{Bmatrix} \tag{10}$$

With A_k and B_k known, the artifact roundness $P(\theta)$ is fully defined. The roundness is then used to determine the spindle error motion $S(\theta)$ as shown in Eq. (11),

$$S(\theta) = m_A(\theta) - P(\theta) \tag{11}$$

This method requires accurate knowledge of the orientation angles ϕ and ψ of the sensors and closely matched sensitivity of the displacement sensors. The sensors must be carefully aligned so that if the spindle were perfect, the only difference in the measurements $m_A(\theta)$, $m_B(\theta)$, and $m_C(\theta)$ would be a phase shift of the roundness. Much work has been done in investigating the effect of the angular spacing of the sensors, which has been shown to control the unwanted suppression of harmonic content in the separated results. For example, when the sensors are spaced evenly, low order harmonics are suppressed. The effect becomes less severe for asymmetric arrangements of ψ and ϕ but never offers complete separation of spindle and roundness errors [21]. Further research using four or more sensors to reduce, but not eliminate, the suppression of harmonics has been published; however, the use of additional sensors introduces additional errors from imperfect alignment and varying sensitivities as well as markedly more complicated post processing [22,23].

Multi-Step Error Separation. Figure 3 shows a schematic of the multi-step error separation method, in which measurements are made for each position as the artifact is indexed N angular increments of ϕ relative to the spindle [24,25]. A single, fixed sensor measures the displacements from the same orientation angle for all angular increments of the artifact. Therefore, each measurement contains the spindle radial error motion and the phase shifted artifact form error.

The analysis of the N measurements, as a function of the spindle rotor angle θ, is straightforward as shown in Eqs. (12) and (13),

$$S(\theta) \cong \frac{1}{N}\sum_{j=1}^{N} m_j(\theta) \tag{12}$$

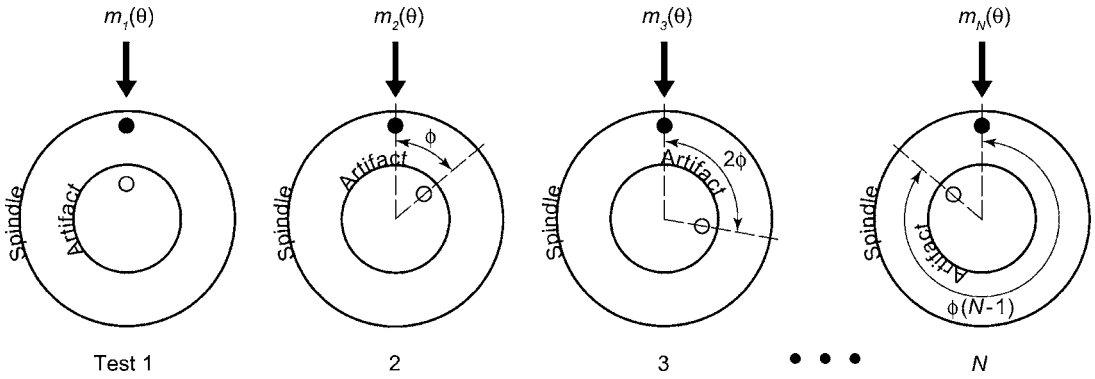

Fig. 3 Schematic of the multi-step error separation method after B89.3.4M [8]

$$P(\theta) = m_1(\theta) - S(\theta) \tag{13}$$

Averaging the multistep measurements separates the error motion of the spindle from the artifact form, except at frequencies that are at integer harmonics of the number of steps. For example, if 12 steps are used in the method, then the spindle and artifact errors occurring at 12 cycles per revolution, 24 cpr, 36 cpr, etc. are not separated. Therefore, caution should be used when interpreting the results. However, when a sufficient number of steps (20, for example) is used, the first distorted harmonic occurs at a relatively high frequency. For high quality lapped artifacts the amplitude of artifact error occurring at these higher harmonics is relatively small (a few nanometers).

Donaldson Reversal. The Donaldson reversal method, which is the rotational equivalent of the well-known straightedge reversal, is shown schematically in Fig. 4. Two measurements $m_F(\theta)$ and $m_R(\theta)$ are recorded, with the artifact and sensor orientation rotated by 180 deg between measurements. This changes the sign of the artifact's form error within the two measurements, enabling the computation of the part profile $P(\theta)$ and spindle error motion $S(\theta)$ using the simple relations in Eqs. (14) and (15)

$$P(\theta) = \frac{m_F(\theta) + m_R(\theta)}{2} \tag{14}$$

$$S(\theta) = \frac{m_F(\theta) - m_R(\theta)}{2} \tag{15}$$

We reported in previous work that a simple modification to the Donaldson's approach greatly improves this reversal method [4,26]. Shown schematically in Fig. 5, a precision rotary table may be used to rotate the spindle stator 180 deg with respect to the displacement sensor which is never moved. A special chuck with a lapped, spherical pilot and precision ground holes is used to index the artifact with an alignment pin sized for a locational interference fit. This modification eliminates repositioning the displacement sensor or any need for multiple sensors. The inherent accuracy of the rotary table is much better (submicrometer) than the accuracy in which sensors can be repositioned and reoriented. Furthermore, the calculations are identical to those of the original method [Eqs. (14) and (15)].

Experimental Setup

The remainder of this paper documents a series of experiments exploring the capability of ultraprecision spindle measurements, including a comparison of results obtained by the multi-step, a multi-probe (3 probes), and the modified-Donaldson reversal approaches to spindle error separation. The test hardware for this research consists of the spindle being tested (test spindle), a rotary encoder, a precision rotary table, a spherical master artifact, a reversal chuck, and a displacement sensor.

The test spindle is an externally pressurized, air bearing spindle (Professional Instruments 4R) with a 4096-count rotary encoder (Heidenhain ERO 1324). Spindle motors and drives can have a significant influence on the synchronous component of the measured data. Our test spindle is examined without a motor, requiring that it be spun up by hand (60 rpm). The encoder is used to trigger the data collection at evenly spaced angular increments in the presence of fluctuations in spindle speed. The spindle is mounted on a precision rotary table (Moore LRT). The reversal chuck between the artifact and spindle has a lapped spherical pilot to facilitate accurate indexing of the artifact with respect to the spindle (Professional Instruments). The rotary table, spindle, reversal chuck, and artifact are assembled such that each component lies on the same axis to within 400 nm. This careful alignment reduces the need for adjustments of the displacement sensor

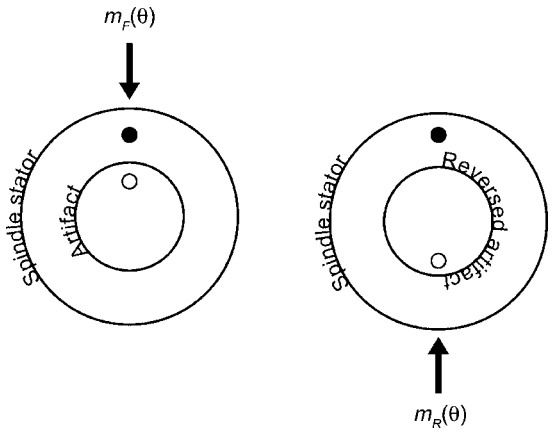

Fig. 4 Schematic of the Donaldson reversal method

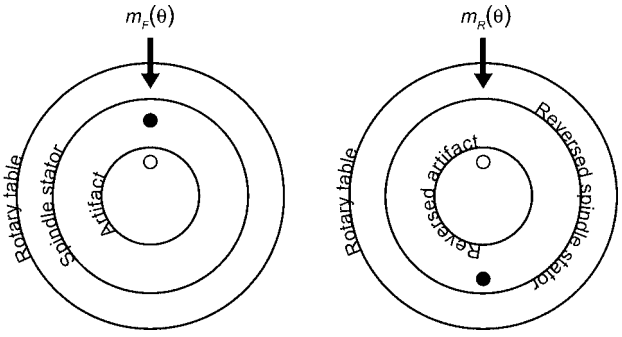

Fig. 5 Schematic of the modified Donaldson reversal method using a precision rotary table and a reversal chuck

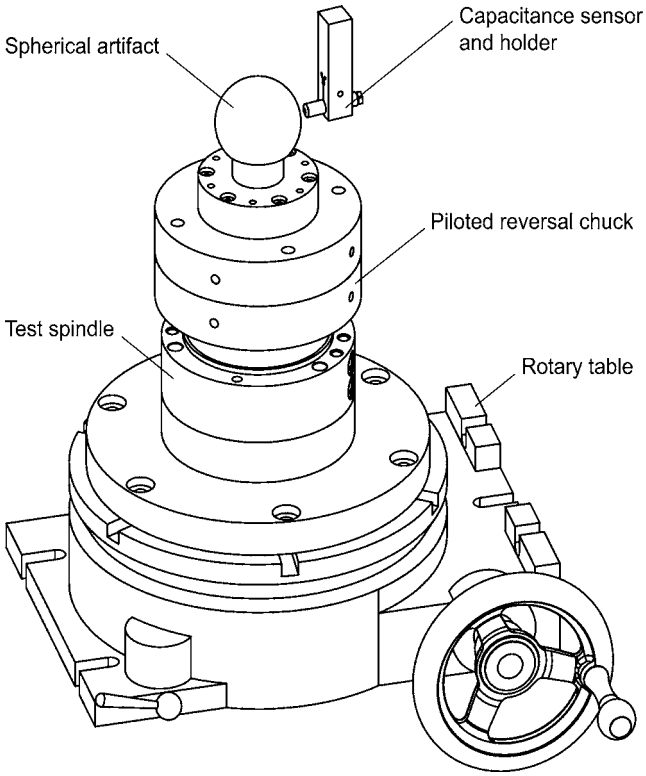

Fig. 6 Spindle test assembly with a spherical master artifact

standoff distance during indexing of the rotary table. The test hardware shown in Fig. 6 is on a three-axis measuring machine (Moore Universal Measuring Machine) to allow for convenient alignment and centering of the displacement sensor (measuring machine not shown in the figure).

The capacitive displacement sensor (Lion Precision C-1C 0.5 nm/mV) targets a ⌀64 mm lapped spherical master artifact (Professional Instruments). Previous work has demonstrated that the finite radius of the artifact results in a slight nonlinearity in the capacitance sensor output. In order to achieve the nanometer-level repeatability results that are shown in the results that follow, it is imperative that the standoff distance of the sensor remain constant during all measurements of a given error separation procedure [27]. For this reason, the electronic zeroing adjustment on the capacitive sensor system is bypassed and the nominal sensor standoff is manually adjusted when necessary.

The data acquisition system (National Instruments PCI-6110E) includes low-pass, analog filters with a 100 Hz cutoff (equivalent to 100 cycles per revolution at 60 rpm) to prevent aliasing and to remove higher frequency spectral content from the data. Additionally, the quasi-static frequency components caused by thermal drift and fluctuations in air bearing supply pressure are removed by high pass digital filtering (0.1 Hz). These procedures are performed in accordance with the B89.3.4M ANSI standard on axis of rotation metrology.

The experimental results are all based on measurements made in the radial direction at the equator of the spherical artifact at an elevation of 187 mm above the geometric center of the test spindle stator. 32 revolutions of data are measured to average out the asynchronous contributions of noise, vibration, and other environmental effects during computation of the synchronous error motion. A single capacitive sensor was used in all measurements and all computations are made using the B89.3.4 definition of a fixed sensitive direction, which is the appropriate measurement for stationary-tool applications such as a lathe (as opposed to a rotating sensitive direction application such as a rotating milling tool).

Table 1 Uncertainty statement for synchronous error motion measurements (32 spindle revolutions) with a fixed sensitive direction (BW 100 Hz) using Donaldson reversal

Uncertainty component	Limit a (nm)	Standard uncertainty u_c (nm)
Displacement sensor		
Internal noise floor	0.2	0.12
Temperature	0.2	0.12
Residual nonlinearity from round target	1.0	0.58
Instrument and structure		
Temperature (after 0.1 cpr high-pass filter)	0.3	0.14
Vibration (after 100 cpr low-pass filter)	0.5	0.29
Bearing air pressure fluctuations	0.3	0.14
Data acquisition		
Board noise	0.1	0.06
Reversal errors		
Rotary table positioning	0.8	0.43
Reversal chuck positioning	0.8	0.43
Combined standard uncertainty (RSS)		1.0 nm
Expanded uncertainty ($k=2$)		2.0 nm

As outlined above, the multi-probe error separation method offers the advantage of simultaneous acquisition of all the necessary measurement data. This benefit must be weighed against the difficulty of precisely aligning three, identical displacement sensors at known angular locations. In our implementation, the three multi-probe measurements are taken using a single sensor by rotating the spindle and artifact on the rotary table. This eliminates the effects of varying sensor sensitivities and also provides accurate and repeatable knowledge of the sensor orientation at the loss of the advantage of simultaneous data acquisition.

Table 1 summarizes the contributors to uncertainty in the measurement of synchronous spindle error motion and artifact form error using the rotary table implementation of Donaldson reversal. The values assigned to the components of uncertainty are based on our tests and experience (Type B evaluation) [28]. A rectangular distribution is assumed for each uncertainty component such that the standard uncertainty u_c is equal to the estimated limit a divided by the square root of three. Grejda provides details on the determination of each of the numerical values of the limits [4]. The combined uncertainty is calculated by the root-sum-of-squares (RSS) method, and a coverage factor of $k=2$ is applied to compute the interval of 95% confidence. Cox and Lazzari discuss additional uncertainty components to be considered in a multi-position error separation scheme [29].

Experimental Results and Discussion

The first experiment establishes the baseline measurement repeatability and only includes the separation of the synchronous and asynchronous components. In this experiment, the spindle stator is never rotated on the rotary table and the artifact remains fixed with respect to the spindle rotor. The plotted results therefore include the combined synchronous spindle radial error motion and the artifact form error, but not disturbances related to physically indexing the spindle and artifact as required by any of the three error separation techniques considered below. Figure 7 shows a polar plot of ten consecutive measurements along with tabulated values of the synchronous (average) and asynchronous runout. These data correspond to $m_A(\theta)$ in the multi-probe, $m_1(\theta)$ in the multi-step, and $m_F(\theta)$ in the Donaldson reversal methods. The synchronous component is computed by taking the average of the data from 32 revolutions of the spindle at each of the 4096 angular measurement locations. The tabulated synchronous error motion

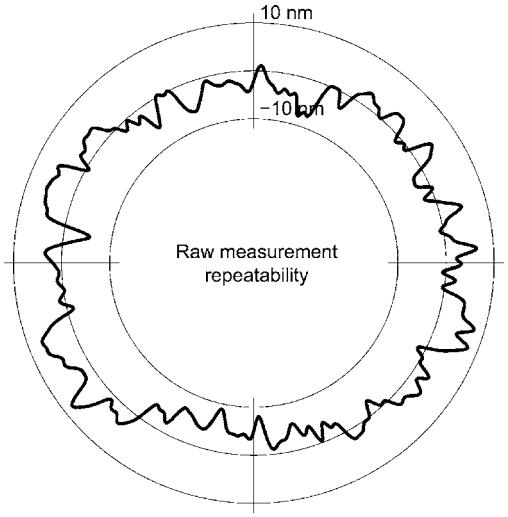

Test	Synchronous	Asynchronous
1	16.9 nm	1.9 nm
2	17.0	1.9
3	17.0	4.6
4	17.0	3.6
5	16.9	1.8
6	17.1	1.4
7	17.0	2.0
8	17.0	1.6
9	17.0	1.4
10	17.0	2.6
Mean	17.0 nm	2.3 nm
Std. dev.	0.07 nm	0.93 nm

Fig. 7 Measurement repeatability without reversal for 10 tests

value is obtained by computing the peak-to-valley range of the 4096 points in the synchronous component. The asynchronous value reported for each test is the peak-to-valley range over all 32 revolutions of the spindle with 4096 points per revolution (131,072 points). The asynchronous value reflects the influence of the spindle plus environmental disturbances, structural vibration and electrical noise from 0.1 to 100 Hz during the 32 revolutions.

The measurement results shown in Fig. 7 demonstrate subnanometer-level repeatability in the measurement of the combined spindle error motion and artifact form error. These are believed to be the most repeatable results published to date.

The second experiment examines the repeatability for the modified (rotary table-based) implementation of Donaldson reversal. Figure 8 shows the repeatability results for the radial synchronous spindle error motion and artifact form error for ten consecutive reversals. In these tests the spindle and artifact results, which are now fully separated from each other, show subnanometer-level repeatability across ten tests.

Having demonstrated that the experimental apparatus and modified Donaldson reversal are repeatable at the subnanometer level, the three error separation methods are now compared for fixed sensitive direction radial error motion and artifact form error obtained by modified Donaldson reversal, a 16-position multistep test, and a 3-probe error separation test. The asynchronous error motion is monitored for every measurement and is consistently between three and five nm, independent of error separation method.

Although the introduction of the rotary table simplifies the execution of the tests, it requires that the measurements be post processed to reflect the changing angular location of the spindle stator. This is because the encoder read head now rotates with respect to the sensor location. In practice, the data are readily indexed to properly account for this modification [4].

The 3-probe error separation calculations are computed using the same data set collected for the 16-step multi-step test with the three sensor positions chosen as 0 deg, 135 deg, and the 247.5 deg. The spacing is deliberately asymmetric to avoid the suppression of low order harmonics in the error motion.

Figures 9 and 10 show the results comparing the three error separation techniques. Figure 9 shows the synchronous radial error motion for all three separation methods on the same plot. These results have been digitally low-pass filtered in post-processing to 15 cycles per revolution. This cutoff frequency is deliberately chosen because it is below the 16 cpr harmonic at which the multi-probe method becomes inaccurate. Figure 9 also shows the discrepancy between the modified Donaldson results and the multi-step results along with the discrepancy between the

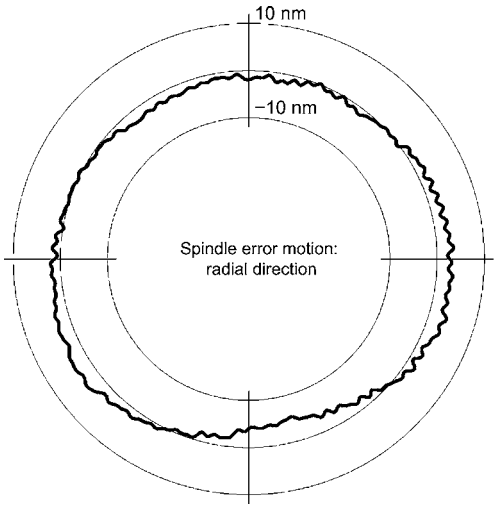

Test	Spindle	Artifact
1	9.1 nm	12.9 nm
2	9.0	12.8
3	9.1	12.9
4	9.2	12.9
5	9.2	12.8
6	9.3	13.0
7	9.3	12.8
8	9.1	12.9
9	9.1	13.0
10	9.2	12.9
Mean	9.2 nm	12.9 nm
Std. dev.	0.09 nm	0.08 nm

Fig. 8 Synchronous spindle error motion (by modified Donaldson reversal) for 10 tests

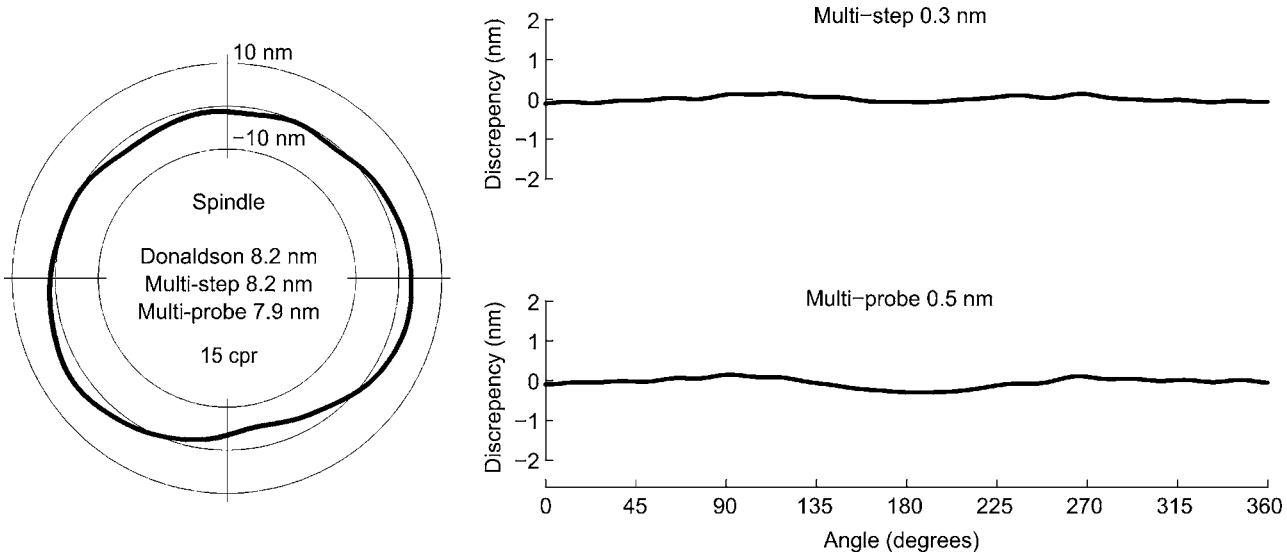

Fig. 9 Error separation results and the discrepancies of multi-step and multi-probe with modified Donaldson reversal (data low-pass filtered to 15 cpr)

modified Donaldson results and the multi-probe results. All three methods give similar values for the error motion to within less than one nanometer.

In Fig. 10, the same results are plotted with a 100 cpr low-pass filter cutoff revealing a more detailed representation of the spindle. As seen in the figure, the multi-probe results no longer match the other two methods because of its inability to separate specific harmonics of the spindle error motion from the artifact form error.

The same information may also be considered in the frequency domain. Figure 11 shows spectral plots of the error motion and artifact form error as computed by the three methods. The three methods agree remarkably well except at the frequencies that have been predicted to be inaccurate in previous work [17,22]. In general, these inaccurate spectral components occur at frequencies that are predicted using the number and angular locations of the sensor used in the multi-position methods.

Conclusion and Discussion

A new experimental apparatus enables the comparison of Donaldson reversal, a multi-probe, and a multi-step method for separating spindle error motion from artifact form error. A new modification to the traditional measurement hardware eliminates two of the largest sources of measurement uncertainty, repositioning sensors and multiple sensor sensitivities, to achieve an expanded uncertainty of 2 nm. This is achieved by using a precision rotary table and a precision reversal chuck to carry out the necessary changes in sensor/target orientation. Analog and digital filtering of the displacement measurements eliminates aliasing, thermal drift, and the effects of structural vibration to yield clean data of a controllable bandwidth.

Three experiments, conducted with a lapped spherical artifact rotating on an externally pressurized air-bearing spindle, demonstrate the repeatability of the displacement measurements (peak-

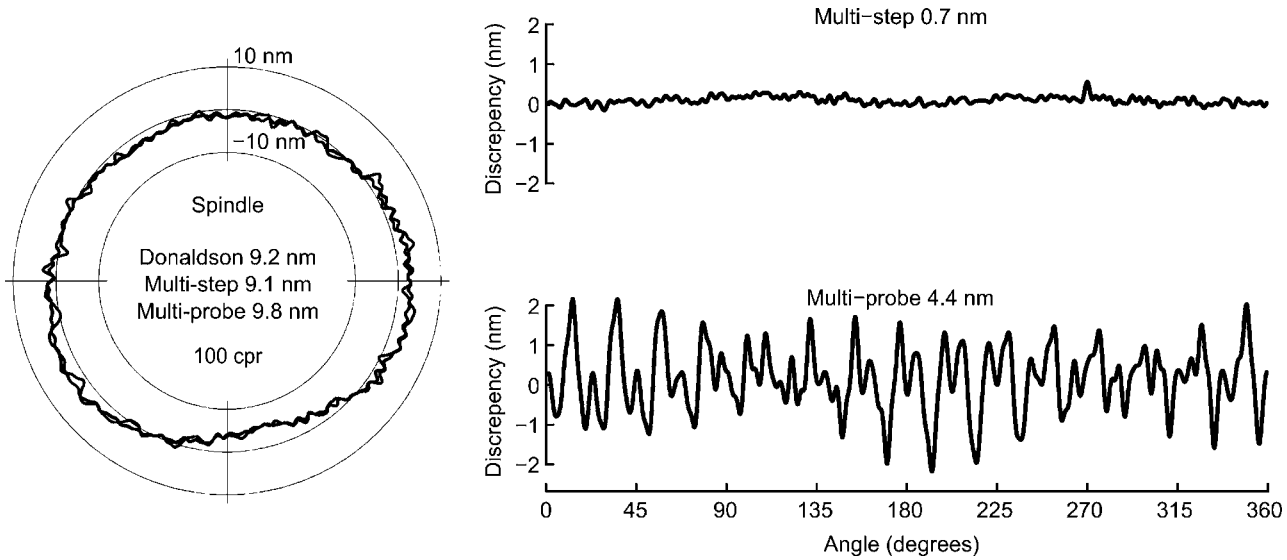

Fig. 10 Error separation results and the discrepancies of multi-step and multi-probe with modified Donaldson reversal (data low-pass filtered to 100 cpr)

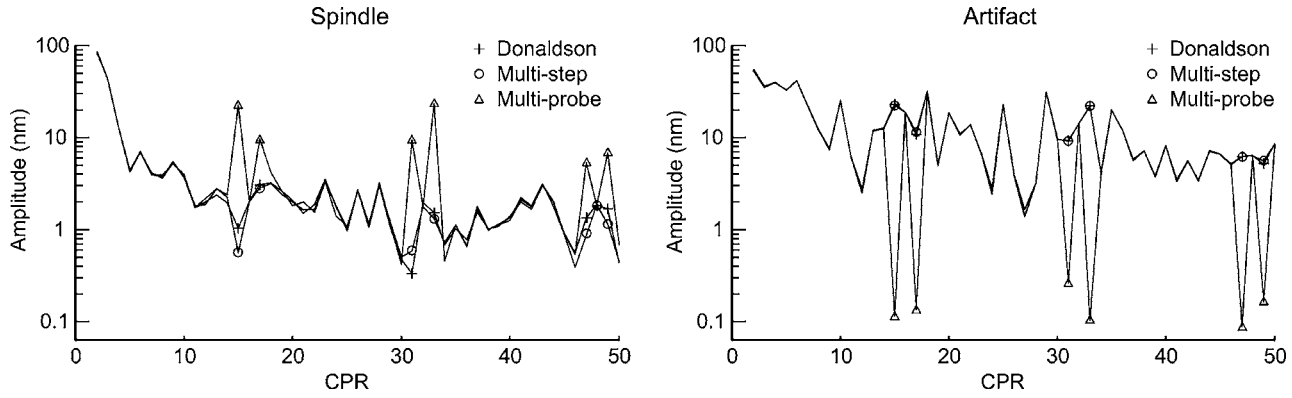

Fig. 11 Frequency components of the three error separation methods

to-valley range of 0.2 nm in 10 tests), the repeatability of Donaldson reversal (*P-V* range of 0.3 nm in 10 tests), and agreement of the three methods (0.3 nm discrepancy between Donaldson reversal and multi-step and 0.5 nm discrepancy between Donaldson and multi-probe when filtered with a 15 cpr low pass cut-off).

In the first experiment, the ten tests demonstrate that the standard deviations of synchronous and asynchronous displacement measurements without error separation are 0.07 nm and 0.93 nm, respectively. In the second experiment, the ten tests demonstrate that conducting the modified Donaldson reversal on this apparatus yields measurements of the radial error motion and the artifact's out-of-roundness that repeat with a standard deviation below 0.1 nm. The final comparison demonstrates that the three methods agree, within their well-documented limitations for not separating certain frequencies, to better than a nanometer. Therefore, the apparatus and techniques described in this paper are well suited for the metrology of high-precision spindles and artifacts at the nanometer level.

References

[1] Taniguchi, N., 1983, "Current Status in, and Future Trends of, Ultraprecision Machining and Ultrafine Materials Processing," CIRP Ann., **32**(2), pp. 573–582.

[2] Bryan, J., Clouser, R., and Holland, E., 1967, "Spindle Accuracy," Am. Mach., **111**(25), pp. 149–164.

[3] Tlusty, J., 1959, "Systems and Methods of Testing Machine Tools," Microtechnic, **13**(4), pp. 162–178.

[4] Grejda, R. D., 2002, "Use and Calibration of Ultraprecision Axes of Rotation With Nanometer Level Metrology," Penn State University, Ph.D. thesis.

[5] Donaldson, R. R., 1972, "A Simple Method for Separating Spindle Error From Test Ball Roundness Error," CIRP Ann., **21**(1), pp. 125–126.

[6] Bryan, J. B., and Vanherck, P., 1975, "Unification of Terminology Concerning the Error Motion of Axes of Rotation," CIRP Ann., **24**(2), pp. 555–562.

[7] Scientific Technical Committee Me, 1976, "Unification Document Me: Axes of Rotation," CIRP Ann., **25**(2), pp. 545–564.

[8] ANSI/ASME B89.3.4M Axes of Rotation: Methods for Specifying and Testing Standard, 1985.

[9] Thompson, D. C., 1982, "Compuron: How Round is Round? LLNL Energy and Technology Review," pp. 1–9.

[10] Vanherck, P., and Peters, J., 1973, "Digital Axis of Rotation Measurement," CIRP Ann., **22**(1), pp. 135–136.

[11] Mitsui, K., 1982, "Development of a New Measuring Method for Spindle Rotation Accuracy by Three Points Method," Proceedings of the 23rd International MTDR Conference, pp. 115–121.

[12] Arora, G. K., Mallanna, C., Anantharaman, B. K., and Babin, P., 1977, "Measurement and Evaluation of Spindle Running Error," Int. J. Mach. Tool Des. Res., **17**(2), pp. 127–135.

[13] Murthy, T. S. R., Mallanna, C., and Visveswaran, M. E., 1978, "New Methods of Evaluating Axis of Rotation Error," CIRP Ann., **27**(1), pp. 365–369.

[14] DeBra, D. B., 1986, "Spindle Metrology—A Student Project," presentation at the SME 7th International Precision Machining and Gaging Symposium.

[15] Chapman, P. D., 1985, "A Capacitance Based Ultra-Precision Spindle Analyzer," J. Jpn. Soc. Precis. Eng., **7**(3), pp. 129–137.

[16] Hansen, H. J., 1988, "A New Dynamic Spindle Analyzer," LLNL Preprint—UCRL 99490.

[17] Whitehouse, D. J., 1976, "Some Theoretical Aspects of Error Separation Techniques in Surface Metrology," J. Phys. E, **9**, pp. 531–536.

[18] Salsbury, J. G., 2003, "Implementation of the Estler Face Motion Reversal Technique," J. Soc. Precis. Eng., **27**(2), pp. 189–194.

[19] Evans, C. J., Hocken, R. J., and Estler, W. T., 1996, "Self-Calibration: Reversal, Redundancy, Error Separation, and Absolute Testing," CIRP Ann., **45**(2), pp. 617–634.

[20] Mitsui, K., 1982, "Development of a New Measuring Method for Spindle Rotation Accuracy by Three Points Method," in Proceedings of the 23rd International MTDR Conference, pp. 115–121.

[21] Moore, D., 1989, "Design Considerations in Multi-probe Roundness Measurement," J. Phys. E, **22**(6), pp. 339–343.

[22] Zhang, G. X., and Wang, R. K., 1993, "Four-Point Method of Roundness and Spindle Error Motion Measurements," CIRP Ann., **42**(1), pp. 593–596.

[23] Zhang, G. X., Zhang, Y. H., Yang, Z. L., and Li, Z., 1997, "A Multipoint Method for Spindle Error Motion Measurement," CIRP Ann., **46**(1), pp. 441–445.

[24] Chetwynd, D. G., and Siddall, G. J., 1976, "Improving the Accuracy of Roundness Measurement," J. Phys. E, **9**(7), pp. 537–544.

[25] Estler, W. T., Evans, C. J., and Shao, L. Z., 1997, "Uncertainty Estimation for Multiposition Form Error Metrology," J. Soc. Precis. Eng., **21**(2-3), pp. 72–82.

[26] Grejda, R. D., Marsh, E. R., and Vallance, R. R., 2005, "Techniques for Calibrating Spindle With Nanometer Error Motion," ASPE Journal of Precision Engineering, **29**(1), pp. 113–123.

[27] Vallance, R. R., Marsh, E. R., and Smith, P. T., 2004, "The Effects of Spherical Target Radius on Capacitive Sensor Measurements," ASME J. Manuf. Sci. Eng., **126**, pp. 822–829.

[28] Taylor, B. N., and Kuyatt, C. E., 1994, "Guidelines for Evaluating and Expressing the Uncertainty of NIST Measurement Results," NIST Technical Note 1297.

[29] Cox, M. G., and Lazzari, A., 2004, "Modelling and Uncertainty for High-Accuracy Roundness Measurement 10th IMEKO TC7 International Symposium," June 30–July 2, 2004, Saint-Petersburg, Russia, pp. 1–5.